

# Analyzing the Scalar Top Co-Annihilation Region at the ILC

M. Carena<sup>1</sup>, A. Finch<sup>2</sup>, A. Freitas<sup>1</sup>, C. Milstène<sup>1</sup>, H. Nowak<sup>3</sup>, A. Sopczak<sup>2</sup>

<sup>1</sup> *Fermi National Accelerator Laboratory, Batavia, IL 60510-500, USA*

<sup>2</sup> *Lancaster University, Lancaster LA1 4YB, United Kingdom*

<sup>3</sup> *Deutsches Elektronen-Synchrotron DESY, D-15738 Zeuthen, Germany*

## Abstract

The Minimal Supersymmetric Standard Model opens the possibility of electroweak baryogenesis provided that the light scalar top quark (stop) is lighter than the top quark. In addition, the lightest neutralino is an ideal candidate to explain the existence of dark matter. For a light stop with mass close to the lightest neutralino, the stop-neutralino co-annihilation mechanism becomes efficient, thus rendering the predicted dark matter density compatible with observations. Such a stop may however remain elusive at hadron colliders. Here it is shown that a future linear collider provides a unique opportunity to detect and study the light stop. The production of stops with small stop-neutralino mass differences is studied in a detailed experimental analysis with a realistic detector simulation including a CCD vertex detector for flavor tagging. Furthermore, the linear collider, by precision measurements of superpartner masses and mixing angles, also allows to determine the dark matter relic density with an accuracy comparable to recent astrophysical observations.

# 1 Introduction

Among the most challenging questions for high energy physics research during the next decades is the origin and stabilization of the mechanism of electroweak symmetry breaking in particle physics and the nature of dark matter and baryogenesis in cosmology. Both aspects suggest the existence of new symmetries within the reach of the next generation of colliders, thereby highlighting an interface between particle physics and cosmology.

The existence of dark matter in the universe has been firmly established by various experiments. Recently the dark matter abundance has been precisely determined by the Wilkinson Microwave Anisotropy Probe (WMAP) [1], in agreement with the Sloan Digital Sky Survey (SDSS) [2],  $\Omega_{\text{CDM}}h^2 = 0.1126_{-0.0181}^{+0.0161}$  at the 95% C.L. Here  $\Omega_{\text{CDM}}$  is the ratio of the dark matter energy density to the critical density  $\rho_c = 3H_0^2/(8\pi G_N)$ , where  $H_0 = h \times 100$  km/s/Mpc is the Hubble constant and  $G_N$  is Newton's constant. One of the most attractive possibilities to explain the nature of dark matter is the existence of weakly interacting massive particles (WIMPs), which are stable due to an additional new symmetry.

Moreover, the generation of the baryon-antibaryon-asymmetry (baryogenesis) in the universe also demands the introduction of new physics beyond the Standard Model. Any mechanism for baryogenesis must fulfill the three Sakharov conditions [3]: (i) the existence of baryon number violating processes, (ii) CP violation and (iii) a departure from thermal equilibrium. Although the three conditions are fulfilled in the Standard Model, the mechanism of electroweak baryogenesis is ruled out. Baryon number violation arises in the Standard Model and extensions thereof in the form of non-perturbative sphaleron processes. Out-of-equilibrium transitions can occur at the electroweak phase transition if it is sufficiently strongly first order,  $v(T_c)/T_c \gtrsim 1$ , where  $v(T_c)$  denotes the Higgs vacuum expectation value at the critical temperature  $T_c$  [4]. A first-order phase transition can be induced by loop contributions of light bosonic particles to the finite temperature Higgs potential, but in the Standard Model the contribution of the gauge bosons is too small to allow for  $v(T_c)/T_c \gtrsim 1$  while obeying the Higgs mass bound from LEP [5]. In addition, CP violation in the Standard Model through the phase in the CKM quark mixing matrix is not sufficient to explain the baryon asymmetry in the universe [6].

One of the most compelling theories for physics beyond the Standard Model is supersymmetry, which stabilizes the difference between the scale of electroweak physics,  $\Lambda_{\text{weak}} \sim 100$  GeV, and the scale of Grand Unified Theories (GUTs),  $\Lambda_{\text{GUT}} \sim 10^{16}$  GeV. The hierarchy stabilization suggests that the masses of the supersymmetric partners of the Standard Model particles are near the TeV scale, within reach of the next generation of colliders. In the presence of  $R$ -parity, which assigns  $R = 1$  to Standard Model particles and  $R = -1$  to their supersymmetric partners, the lightest supersymmetric particle (LSP) is stable and provides a natural dark matter candidate.

In the Minimal Supersymmetric extension of the Standard Model (MSSM), the superpartners of the top quark, the scalar top quarks (stops), have an important impact on the Higgs potential [7–10]. Loop effects of light stops can induce a strongly first order electroweak phase transition, thus generating the out-of-equilibrium condition for electroweak baryogenesis. In addition, supersymmetric models offer new sources of CP violation to explain the

magnitude of the baryon asymmetry.

To open the window for electroweak baryogenesis, the lightest stop mass is required to be smaller than the top quark mass, whereas the Higgs boson involved in the electroweak phase transition must be lighter than about 120 GeV [7–10]. Hence there is an interesting region of parameter space for which the light stop is only slightly heavier than the neutralino LSP, thus implying that the stop-neutralino co-annihilation process becomes significant. In the stop-neutralino co-annihilation region consistent with the measured dark matter value, the mass difference between the light stop and the lightest neutralino is smaller than about 30 GeV [11].

The Tevatron and the Large Hadron Collider (LHC) experiments will be able to probe a light Higgs boson with Standard-Model-like couplings to the gauge bosons, as required by electroweak baryogenesis, but the stop parameter region compatible with dark matter is very difficult to explore at hadron colliders. Preliminary studies for the Tevatron show that with 2–4 fb<sup>-1</sup> of integrated luminosity, stops with masses up to about 170 GeV may be detected if the stop-neutralino mass difference is larger than 30–50 GeV [12]. Smaller mass differences cannot be covered due to the reliance on a trigger for the signature of missing transverse energy. So far, no dedicated studies for light stop exist for the Large Hadron Collider (LHC). However, limitations due to background levels and detector thresholds will be even more severe at the LHC than at the Tevatron<sup>1</sup>.

A future international  $e^+e^-$  linear collider (ILC) provides a clean environment with relatively small background levels that allows the study of stops for small stop-neutralino mass differences. For instance, the Large Electron-Positron Collider (LEP) was able to set limits on the stops even for a mass difference to the neutralino close to 1 GeV [13]. Based on the experience from LEP, the ILC might be able to explore mass differences down to a few GeV even for stop masses comparable with the top quark mass. In the region of parameters where stop-neutralino co-annihilation leads to a value of the relic density consistent with experimental results, the stop-neutralino mass difference is never much smaller than 15 GeV, and hence an ILC seems well suited to explore this region efficiently.

In addition to establishing the existence of light stop quarks, the precise measurement of their properties is crucial for testing their impact on the dark matter relic abundance and the mechanism of electroweak baryogenesis. The relevance of a linear collider to probe MSSM baryogenesis through the chargino sector have been discussed in Ref. [14]. A linear collider provides an excellent environment to perform precise measurements of the stop [15, 16] and chargino systems [17, 18].

In this work it is shown that the ILC offers a unique possibility to elucidate the scenario of light stop quarks and its cosmological implications. The capabilities of the ILC for searching stops with small stop-neutralino mass differences is investigated in detail, including realistic detector simulations. It is studied to which accuracy the stop mass, mixing angle and stop-neutralino mass difference can be determined at the ILC, also under the presence of potential CP phases. This involves the analysis of the decay spectra and production cross-sections for

---

<sup>1</sup>However, at the LHC, the production of stops from gluino decays,  $pp \rightarrow \tilde{g}\tilde{g} \rightarrow tt\tilde{t}^*\tilde{t}^*$ , with same-sign leptonic tagging of the top quarks, might offer additional prospect for studying stops for small mass differences. This channel is currently under study.

different beam polarizations. From the expected accuracies at the ILC, we will furthermore explore how precisely the contribution of stop co-annihilation to the dark matter relic density can be computed.

After introducing the relevant notations and theoretical constraints and assumptions for the light stop scenario in section 2, an experimental study for stop searches at the linear collider is presented in section 3. Section 4 analyzes the achievable precision for the determination of the underlying supersymmetric parameters, which is used in section 5 to derive the expected accuracy for the computation of the dark matter density from linear collider measurements. The final conclusions are given in section 6.

## 2 Notation and conventions

This work is restricted to the framework of the Minimal Supersymmetric Standard Model (MSSM), including CP-violating phases in the supersymmetry breaking terms.

Since the Yukawa couplings of the first two generations are very small, mixing between the L- and R-sfermions, partners of the left- and right-handed fermions, of the first two generations can be neglected. For the supersymmetric partners of the top quark, the scalar top quark (stop), on the other hand, mixing effects are very important. The stop mass matrix is given by

$$M_{\tilde{t}}^2 = \begin{pmatrix} m_{\tilde{Q}_3}^2 + m_t^2 + \left(\frac{1}{2} - \frac{2}{3}s_W^2\right)m_Z^2 \cos 2\beta & m_t(A_t^* - \mu \cot \beta) \\ m_t(A_t - \mu^* \cot \beta) & m_{\tilde{U}_3}^2 + m_t^2 + \frac{2}{3}s_W^2 m_Z^2 \cos 2\beta \end{pmatrix}, \quad (1)$$

where  $\tan \beta$  is the ratio of the vacuum expectation values of the two Higgs doublets,  $m_{\tilde{Q}_3}$ ,  $m_{\tilde{U}_3}$  are the left- and right-chiral stop supersymmetry breaking masses, respectively,  $A_t$  is the trilinear stop soft breaking parameter and  $\mu$  is the Higgs/higgsino parameter in the superpotential. Diagonalization of the stop mass matrix yields the mass eigenvalues

$$m_{\tilde{t}_{1,2}}^2 = \frac{1}{2} \left[ M_{\tilde{t},11}^2 + M_{\tilde{t},22}^2 \mp \sqrt{\left(M_{\tilde{t},11}^2 - M_{\tilde{t},22}^2\right)^2 + 4|M_{\tilde{t},12}|^4} \right], \quad (2)$$

and the mixing angle

$$\sin^2 \theta_{\tilde{t}} = \frac{|M_{\tilde{t},12}|^4}{2|M_{\tilde{t},12}|^4 + (m_{\tilde{t}_1}^2 - M_{\tilde{t},22}^2)(M_{\tilde{t},11}^2 - M_{\tilde{t},22}^2)}. \quad (3)$$

In this work, inter-generational (CKM) mixing effects for fermions and sfermions are neglected.

Apart from the electroweak parameters, the spectrum of the charginos and neutralinos is described by the Higgs/higgsino parameter  $\mu$  and the soft SU(2) and U(1) gaugino parameters,  $M_2$  and  $M_1$ , respectively. In the wino-higgsino basis, the chargino mass matrix reads

$$X = \begin{pmatrix} M_2 & \sqrt{2}m_W \sin \beta \\ \sqrt{2}m_W \cos \beta & \mu \end{pmatrix}. \quad (4)$$

The mass eigenvalues and the mixing angles for the left- and right-chiral chargino components are obtained according to [18]

$$m_{\tilde{\chi}_{1,2}^\pm}^2 = \frac{1}{2} (M_2^2 + |\mu|^2 + 2m_W^2 - \Delta_C), \quad (5)$$

$$\cos 2\phi_{L,R} = -(M_2^2 - |\mu|^2 \mp 2m_W^2 \cos 2\beta) / \Delta_C. \quad (6)$$

with

$$\Delta_C = \sqrt{(M_2^2 - |\mu|^2)^2 + 4m_W^4 \cos^2 2\beta + 4m_W^2 (M_2^2 + |\mu|^2) + 8m_W^2 M_2 |\mu| \sin 2\beta \cos \phi_\mu}. \quad (7)$$

The neutralino mass term in the current eigen-basis is given by

$$\mathcal{L}_{m_{\tilde{\chi}^0}} = -\frac{1}{2} \psi^{0\top} Y \psi^0 + \text{h.c.}, \quad \psi^0 = (\tilde{B}, \tilde{W}^0, \tilde{H}_d^0, \tilde{H}_u^0)^\top, \quad (8)$$

with the symmetric mass matrix

$$Y = \begin{pmatrix} M_1 & 0 & -m_Z s_W c_\beta & m_Z s_W s_\beta \\ 0 & M_2 & m_Z c_W c_\beta & -m_Z c_W s_\beta \\ -m_Z s_W c_\beta & m_Z c_W c_\beta & 0 & -\mu \\ m_Z s_W s_\beta & -m_Z c_W s_\beta & -\mu & 0 \end{pmatrix}, \quad (9)$$

in which the abbreviations  $s_\beta = \sin \beta$  and  $c_\beta = \cos \beta$  have been introduced;  $s_W$  and  $c_W$  are the sine and cosine of the electroweak mixing angle. The transition to the mass eigen-basis is performed by the unitary mixing matrix  $N$ ,

$$N^* Y N^{-1} = \text{diag}(m_{\tilde{\chi}_1^0}^2, m_{\tilde{\chi}_2^0}^2, m_{\tilde{\chi}_3^0}^2, m_{\tilde{\chi}_4^0}^2). \quad (10)$$

Explicit analytical solutions for the mixing matrices can be found in Ref. [18, 20]<sup>2</sup>.

In the MSSM Higgs sector, the tree-level masses of the CP-even neutral Higgs bosons  $h^0$  and  $H^0$  and the charged scalar  $H^\pm$  can be expressed through the gauge boson masses, the mass of the pseudo-scalar Higgs boson,  $m_{A^0}$ , and  $\tan \beta$ . The Born relations are however significantly modified by radiative corrections, with dominant effects originating from top and stop loops.

In the MSSM the Higgs mass is very sensitive to the stop spectrum. In order to be consistent with the bound  $m_{h^0} \gtrsim 114.4$  GeV from direct searches at LEP [21] and with one light stop state, the heavier stop mass has to be above about 1 TeV and the trilinear coupling  $A_t$  has to be sizable [9]. Constraints from electroweak precision data are satisfied when the light stop is mainly right-chiral. This is naturally achieved for values of the stop supersymmetry breaking parameters  $m_{\tilde{Q}_3}^2 \gtrsim 1 \text{ TeV}^2$  and  $m_{\tilde{U}_3}^2 \lesssim 0$ , respectively. The stop mixing parameter  $X_t = \mu \cot \beta - A_t$  is bounded from below by the Higgs boson mass constraint from LEP and from above by the requirement of the strength of the first order

---

<sup>2</sup>Note that the convention for the chargino mass matrix  $X$  used in Ref. [18] is different from eq. (4).

electroweak phase transition, leaving the allowed range  $0.3 \lesssim |X_t|/m_{\tilde{Q}_3} \lesssim 0.5$  [9]. The lower bound is weakened for large values of  $m_{\tilde{Q}_3}$  of several TeV.

The MSSM Higgs masses with CP violation have been calculated including complete one-loop and leading two-loop corrections, see *e.g.* Ref. [22]. In this work, however, the process of baryogenesis at the electroweak phase transition is computed with the program of Refs. [23, 24], which includes only one-loop corrections to the zero temperature Higgs potential. Since the allowed mass range for the Higgs boson is constrained by the mechanism of electroweak baryogenesis, for consistency the Higgs mass is determined by the minimization of the one-loop effective potential. This implies that only one-loop corrections are included in the calculation of the Higgs mass as well<sup>3</sup>.

For successful electroweak baryogenesis, an additional source of CP violation beyond the Standard Model CKM matrix is necessary. Within the MSSM, the dominant source are chargino loops, with a contribution proportional to  $\text{Im}\{\mu M_2\}$  [23, 26]. To generate a sufficiently large baryon asymmetry, the charginos are required to be relatively light,  $m_{\tilde{\chi}_1^\pm} \sim \mathcal{O}(\text{a few } 100 \text{ GeV})$ . In addition, the CP-violating phase needs to be sizable,  $\arg(\mu M_2) \gtrsim 0.1$  [23].

A very large CP-violating phase, on the other hand, is restricted by experimental bounds on the electric dipole moments of the electron, neutron and  $^{199}\text{Hg}$  nucleus. The leading contributions from one-loop sfermion-gaugino loops [27, 28] become small for large masses of the first two generation sfermions of several TeV. Furthermore, CP-violating phases in the sfermion  $A$ -parameters can result in cancellations for the electric dipole moments [27], without having much effect on electroweak baryogenesis. For the present work, the strongest constraint arises from the bound on the electric dipole moment of the electron,  $|d_e| < 1.6 \times 10^{-27} e \text{ cm}$  [29], effectively restricting the allowed MSSM parameter space.

A CP-violating phase in  $M_2$  can always be transferred into the  $\mu$  parameter by means of a unitary transformation. In principle, there can also be non-trivial phases in the gaugino parameters  $M_1$  and  $M_3$ , but their effect on electroweak baryogenesis is small. Therefore in the following all gaugino soft parameters are assumed real, while the generation of the baryon asymmetry is connected with a phase in the  $\mu$  parameter,

$$\mu = |\mu| \times e^{i\phi_\mu}. \quad (11)$$

For simplicity, this report will only investigate scenarios where the lightest neutralino is bino-like, *i.e.*  $M_1 \ll M_2, |\mu|$  and the annihilation cross-section is importantly enhanced through co-annihilation with the stop. For small values of  $\mu$ , the LSP can acquire a significant Higgsino component, which increases the annihilation via s-channel  $Z$  and Higgs boson exchange. This case will be considered elsewhere.

### 3 Analysis of light stops at a linear collider

For small mass differences  $\Delta m = m_{\tilde{t}_1} - m_{\tilde{\chi}_1^0}$ , the dominant decay mode of the light stop quark,  $m_{\tilde{t}_1} < m_t$ , is into a charm quark and the lightest neutralino,  $\tilde{t}_1 \rightarrow c \tilde{\chi}_1^0$ . In the parameter

<sup>3</sup>An analysis including two-loop corrections to the effective potential is in progress [25].

region where the co-annihilation mechanism becomes efficient, the typical mass differences are  $\Delta m < 30$  GeV. Thus the two- and three-body decay modes  $\tilde{t}_1 \rightarrow t \tilde{\chi}_1^0$ ,  $\tilde{t}_1 \rightarrow b \tilde{\chi}_1^+$ ,  $\tilde{t}_1 \rightarrow b W^+ \tilde{\chi}_1^0$  and  $\tilde{t}_1 \rightarrow b l^+ \tilde{\nu}_l$  are kinematically forbidden, since the sneutrino and chargino are assumed to be heavier than the light stop. Since the decay  $\tilde{t}_1 \rightarrow c \tilde{\chi}_1^0$  occurs only at one-loop order, it is formally of the same order  $\mathcal{O}(\alpha^3)$  as the four-body decay  $\tilde{t}_1 \rightarrow b l^+ \nu_l \tilde{\chi}_1^0$ . However, the decay into a charm quark is sensitive to the supersymmetric flavor structure at the supersymmetry breaking scale [30]. For models with high-scale supersymmetry breaking, this therefore introduces a large enhancement factor for this process. In the following it is assumed that the branching ratio for  $\tilde{t}_1 \rightarrow c \tilde{\chi}_1^0$  is 100%.

In this section the production of light stops at a  $\sqrt{s} = 500$  GeV linear collider is analyzed. The analysis makes use of high luminosity  $\mathcal{L} \sim 500 \text{ fb}^{-1}$  and polarization of both beams. At an  $e^+e^-$  collider, scalar top quarks could be produced in pairs,

$$e^+e^- \rightarrow \tilde{t}_1 \tilde{t}_1^* \rightarrow c \tilde{\chi}_1^0 \bar{c} \tilde{\chi}_1^0, \quad (12)$$

leading to a signature of two charm jets plus missing energy. The tree-level cross-section reads

$$\sigma[e^+e^- \rightarrow \tilde{t}_1 \tilde{t}_1^*] = \frac{\pi \alpha^2}{2s} (1 - 4m_{\tilde{t}_1}^2/s)^{3/2} \sum_{i=L,R} P_i \left[ \frac{2}{3} + g_i \frac{3 \cos^2 \theta_t - 4s_W^2}{6s_W c_W} \frac{s}{s - m_Z^2} \right]^2, \quad (13)$$

with

$$g_L = \frac{-1 + 2s_W^2}{2s_W c_W}, \quad g_R = \frac{s_W}{c_W}, \quad P_{L,R} = [1 \mp P(e^-)] [1 \pm P(e^+)], \quad (14)$$

where  $P(e^\pm)$  are the polarization degrees of the  $e^\pm$  beams and negative/positive values indicate left-/right-handed polarization.

For small  $\Delta m$ , the jets are relatively soft and it is challenging to separate them from Standard Model backgrounds. Since small differences in the expected signal and background distributions contribute to the selection of the signal events, a realistic detector simulation is applied. Both the signal and background events are generated with PYTHIA 6.129 [31], which has been adapted with a private code for the stop signal generation [32] and preselection previously used in Ref. [16]. The SIMDET detector simulation [33] has been used, describing a typical ILC detector. The analysis is based on the tool N-TUPLE [34], which incorporates jet finding algorithms. The cross-sections of the signal process and the relevant background processes have been computed by adapting the Monte-Carlo code used in Ref. [35] and by GRACE 2.0 [36], with cross-checks with COMPHEP 4.4 [37] for most processes. Table 1 summarizes the expected signal and background cross-sections. To avoid the infrared divergence of the two-photon background, it is given with a cut on the minimal transverse momentum,  $p_t > 5$  GeV.

All processes are simulated including beamstrahlung for cold ILC technology as parameterized in the program CIRCE 1.0 [38]. The effect of beamstrahlung is twofold. Firstly, due to electromagnetic interactions between the two densely charged incoming bunches, a spread of the  $e^+/e^-$  beam energy spectra is generated. On the other hand, these electromagnetic interactions result in the radiation of (typically soft) photons that can interact and lead to

Process	Cross-section [pb]		
	0/0	-80%/+60%	+80%/-60%
$P(e^-)/P(e^+)$			
$\tilde{t}_1\tilde{t}_1^*$ $m_{\tilde{t}_1} = 120$ GeV	0.115	0.153	0.187
$m_{\tilde{t}_1} = 140$ GeV	0.093	0.124	0.151
$m_{\tilde{t}_1} = 180$ GeV	0.049	0.065	0.079
$m_{\tilde{t}_1} = 220$ GeV	0.015	0.021	0.026
$W^+W^-$	8.55	24.54	0.77
$ZZ$	0.49	1.02	0.44
$We\nu$	6.14	10.57	1.82
$eeZ$	7.51	8.49	6.23
$q\bar{q}, q \neq t$	13.14	25.35	14.85
$t\bar{t}$	0.55	1.13	0.50
2-photon, $p_t > 5$ GeV	936		

**Table 1:** Cross-sections for the stop signal and Standard Model background processes for  $\sqrt{s} = 500$  GeV and different polarization combinations. The signal is given for  $\cos\theta_{\tilde{t}} = 0.5$  and different values of the stop mass. Negative polarization values refer to left-handed polarization and positive values to right-handed polarization.

two-photon events in addition to the normal two-photon background mentioned above. In Table 1, the combined two-photon background from all sources is listed.

As evident from the table, the Standard Model backgrounds are several orders of magnitude larger than the signal and need to be reduced with efficient selection cuts. Backgrounds from supersymmetric processes are typically small [16]. If the stop is very light and the light chargino can decay into the stop and a bottom quark,  $\tilde{\chi}_1^+ \rightarrow \tilde{t}_1 \bar{b}$ , the largest supersymmetric background comes from chargino pair production. Although this process has a four-jet signature with two b-quark jets and two c-quark jets, a fraction of events with overlapping jets can be a relevant background to stop pair production, since the chargino production cross-section is typically large, of the order of 1 pb.<sup>4</sup> The contribution of this background will be addressed later in this section.

In the first step of the event selection, the following preselection cuts are applied:

$$\begin{aligned}
4 < N_{\text{charged tracks}} < 50, & \quad p_t > 5 \text{ GeV}, \\
|\cos\theta_{\text{thrust}}| < 0.8, & \quad |p_{\text{long,tot}}/p_{\text{tot}}| < 0.9, \\
E_{\text{vis}} < 0.75\sqrt{s}, & \quad m_{\text{inv}} < 200 \text{ GeV}.
\end{aligned} \tag{15}$$

The lower cut on the number of charged tracks removes most of the background with leptons and no jets and the upper cut part of the  $t\bar{t}$  background. By requiring a minimal transverse

---

<sup>4</sup>Depending on the supersymmetry scenario, chargino pair production can actually be an interesting discovery process for light stops. However, this possibility will not be explored further in this paper.



Process	Total	After presel.	cut 1	cut 2	cut 3	cut 4	cut 5	cut 6	Scaled to 500 fb <sup>-1</sup>
$W^+W^-$	210,000	2814	827	28	25	14	14	8	145
$ZZ$	30,000	2681	1987	170	154	108	108	35	257
$W e \nu$	210,000	53314	38616	4548	3787	1763	1743	345	5044
$eeZ$	210,000	51	24	20	11	6	3	2	36
$q\bar{q}, q \neq t$	350,000	341	51	32	19	13	10	8	160
$t\bar{t}$	180,000	2163	72	40	32	26	26	25	38
2-photon	$8 \times 10^6$	4061	3125	3096	533	402	0	0	< 164
$m_{\tilde{t}_1} = 140$									
$\Delta m = 20$	50,000	68.5	48.8	42.1	33.4	27.9	27.3	20.9	9720
$\Delta m = 40$	50,000	71.8	47.0	40.2	30.3	24.5	24.4	10.1	4700
$\Delta m = 80$	50,000	51.8	34.0	23.6	20.1	16.4	16.4	10.4	4840
$m_{\tilde{t}_1} = 180$									
$\Delta m = 20$	25,000	68.0	51.4	49.4	42.4	36.5	34.9	28.4	6960
$\Delta m = 40$	25,000	72.7	50.7	42.4	35.5	28.5	28.4	20.1	4925
$\Delta m = 80$	25,000	63.3	43.0	33.4	29.6	23.9	23.9	15.0	3675
$m_{\tilde{t}_1} = 220$									
$\Delta m = 20$	10,000	66.2	53.5	53.5	48.5	42.8	39.9	34.6	2600
$\Delta m = 40$	10,000	72.5	55.3	47.0	42.9	34.3	34.2	24.2	1815
$\Delta m = 80$	10,000	73.1	51.6	42.7	37.9	30.3	30.3	18.8	1410

**Table 2:** Total number of events generated for background and signal as well as background event numbers and  $\tilde{t}_1\tilde{t}_1^*$  signal efficiencies in % (for some examples of  $m_{\tilde{t}_1}$  and  $\Delta m$  in GeV) after preselection and each of the final selection cuts. In the last column the expected event numbers are scaled to a luminosity of 500 fb<sup>-1</sup>, for zero beam polarization. The cuts are explained in the text.

momentum  $p_t$ , the two-photon background and back-to-back processes like  $q\bar{q}$  are largely reduced. Since for most background processes a potential momentum or energy imbalance occurs from particles lost in the beam pipe cone, a cut on the thrust angle  $\theta_{\text{thrust}}$  and the longitudinal momentum  $p_{\text{long,tot}}$  reduces all backgrounds. The signal, on the other hand, has very little longitudinal thrust since it follows a polar  $\sin^2\theta$  distribution. Furthermore, the signal is characterized by a large amount of missing energy, corresponding to visible energy  $E_{\text{vis}}$  substantially smaller than the center-of-mass energy. The requirement of missing energy mostly reduces processes without neutrinos in the final state, *i.e.*  $q\bar{q}$  and hadronic decays of  $W^+W^-$ ,  $ZZ$ ,  $t\bar{t}$ . Finally, demanding that the total visible invariant mass is below 200 GeV decreases  $W^+W^-$ ,  $q\bar{q}$  and  $t\bar{t}$  backgrounds without affecting the signal, which typically leads to relatively soft events for small mass differences  $\Delta m$ .

Table 2 shows the number of events generated for each background process and the number of events left after these preselection cuts. Also shown is the efficiency of the signal after the preselection for various values of the stop and neutralino masses. About 70% of the signal events pass the preselection for most of the investigated stop masses and mass differences  $\Delta m$ .

For the final event selection the following cuts are applied (see Table 2):

1. The number of reconstructed jets is required to be exactly two. Jets are reconstructed with the Durham algorithm with the jet resolution parameter  $y_{\text{cut}} = 0.003 \times \sqrt{s}/E_{\text{vis}}$ . As noted in Ref. [39], the  $E_{\text{vis}}$ -dependent  $y_{\text{cut}}$  parameter is crucial for effective di-jet reconstruction over a wide range of stop and neutralino parameters. The coefficient 0.003 was tuned to most effectively reject four-jet  $W^+W^-$  events while preserving most of the signal. The cut reduces substantially the number of  $W$  and quark pair events.
2. The limit on the visible energy  $E_{\text{vis}}$  in the preselection is lowered to  $E_{\text{vis}} < 0.4\sqrt{s}$  in order to cut down on  $W^+W^-$ ,  $ZZ$  and di-quark events. In addition, a window for the invariant jet mass around the  $W$ -boson mass,  $70 \text{ GeV} < m_{\text{jet,inv}} < 90 \text{ GeV}$ , is excluded to reduce the large  $W e \nu$  background.
3. The acollinearity  $\phi_{\text{acol}}$  is defined as the opening angle between the two jets. Events from  $e^+e^- \rightarrow q\bar{q}$  and  $\gamma\gamma \rightarrow q\bar{q}$  processes with back-to-back topology are removed by requiring  $\cos \phi_{\text{acol}} > -0.9$ .
4. By applying a more severe cut on the thrust angle than in the preselection,  $|\cos \theta_{\text{thrust}}| < 0.7$ , events with  $W$  bosons are further reduced.
5. The remaining two-photon background is almost completely removed by increasing the cut on the transverse momentum,  $p_t > 12 \text{ GeV}$ .
6. At this point, the largest remaining background is from single  $W$  production,  $e^+e^- \rightarrow W e \nu$ . It resembles the signal closely in most distributions, *e.g.* as a function of the visible energy, thrust or acollinearity. The only distinctive kinematical discrimination is through the invariant mass distribution, which has a resonance around the  $W$ -boson mass. In addition, the use of charm tagging helps to improve the signal-to-background ratio. Here, the charm tagging is implemented using a neural network analysis as described in Ref. [40]. The neural network has been optimized to single out the desired two-charm events by training it to efficiently reduce the  $W e \nu$  background while preserving the stop signal for small mass differences. For each event, it yields a probability that this event contains two relatively soft charm jets. Only events with an identification probability of more than 40% are kept. Since the charm tagging alone is not sufficient to fully reduce the single- $W$  background, the excluded invariant jet mass window from cut 2 is increased to ( $60 \text{ GeV} < m_{\text{jet,inv}} < 90 \text{ GeV}$ ), at the cost of losing a substantial amount of the signal for certain values of the stop and neutralino masses.

All cuts have been optimized to preserve signal events for small mass differences. The resulting numbers of events, scaled to a luminosity of  $500 \text{ fb}^{-1}$ , and the signal efficiencies

$\Delta m$	$m_{\tilde{t}_1} = 120$ GeV	140 GeV	180 GeV	220 GeV
80 GeV		10%	15%	19%
40 GeV		10%	20%	24%
20 GeV	17%	21%	28%	35%
10 GeV	19%	20%	19%	35%
5 GeV	2.5%	1.1%	0.3%	0.1%

**Table 3:** Signal efficiencies for  $\tilde{t}_1\tilde{t}_1^*$  production after final event selection for different combinations of the stop mass  $m_{\tilde{t}_1}$  and mass difference  $\Delta m = m_{\tilde{t}_1} - m_{\tilde{\chi}_1^0}$ .

are summarized in Table 2. After the final selection, between 10% and 35% of the signal is remaining. The expected  $\tilde{t}_1\tilde{t}_1^*$  signal event numbers are of same order of magnitude as for the Standard Model background,  $N \sim \mathcal{O}(10^4)$ .

As mentioned above, if the stop is lighter than the light chargino, a potentially large background can originate from chargino pair production, with the subsequent decay  $\tilde{\chi}_1^+ \rightarrow \tilde{t}_1 \bar{b}$ . Since this background is characterized by four partons in the final state including two bottom quarks, it is largely removed by the selection of two-jet events and the charm tagging. After applying all cuts listed above, the chargino background is reduced by a factor of about 5000, corresponding to about 100 remaining events for  $500 \text{ fb}^{-1}$  luminosity. It will therefore be neglected in the following.

In order to explore the reach of a future linear collider for very small mass differences  $\Delta m = m_{\tilde{t}_1} - m_{\tilde{\chi}_1^0}$ , signal event samples have been generated also for  $\Delta m = 10$  GeV and 5 GeV. The results are listed in Table 3. As evident from the table, the efficiency drastically deteriorates for  $\Delta m = 5$  GeV, as a result of the  $p_t$  cut (cut 5). An optimization of the event selection for very small mass differences will be addressed in a future study.

Based on the results for residual background levels and signal efficiencies from the experimental simulations, the discovery reach of a 500 GeV  $e^+e^-$  collider can be estimated. Figure 1 shows the discovery reach in the parameter plane of  $m_{\tilde{t}_1}$  and  $m_{\tilde{\chi}_1^0}$ . The signal efficiencies for the parameter points Table 3 are interpolated to cover the whole parameter region of interest. Then, the signal rates are computed from the production cross-section  $\sigma$  for each combination  $(m_{\tilde{t}_1}, m_{\tilde{\chi}_1^0})$ , multiplied by the efficiency  $\epsilon$  obtained from the simulations and the luminosity  $\mathcal{L}$ , resulting in the expected signal event number  $S = \epsilon\mathcal{L}\sigma$ . Together with the number of background events  $B$ , this yields the significance  $S/\sqrt{S+B}$ . The dark shaded (green) area in the figure corresponds to the region where a discovery with five standard deviations is possible,  $S/\sqrt{S+B} > 5$ .

In Fig. 1, the region consistent with baryogenesis and the dark matter abundance measured by WMAP is indicated by the dark gray points. Here the higher density of points at the upper edge of this region corresponds to the area where stop-neutralino co-annihilation is effective, extending to mass differences  $\Delta m$  of about 15 GeV. A linear collider could find light stop quarks for mass differences down to  $\Delta m \sim \mathcal{O}(5 \text{ GeV})$ , covering the complete co-annihilation region. The right plot in Fig. 1 shows that even a relatively small integrated

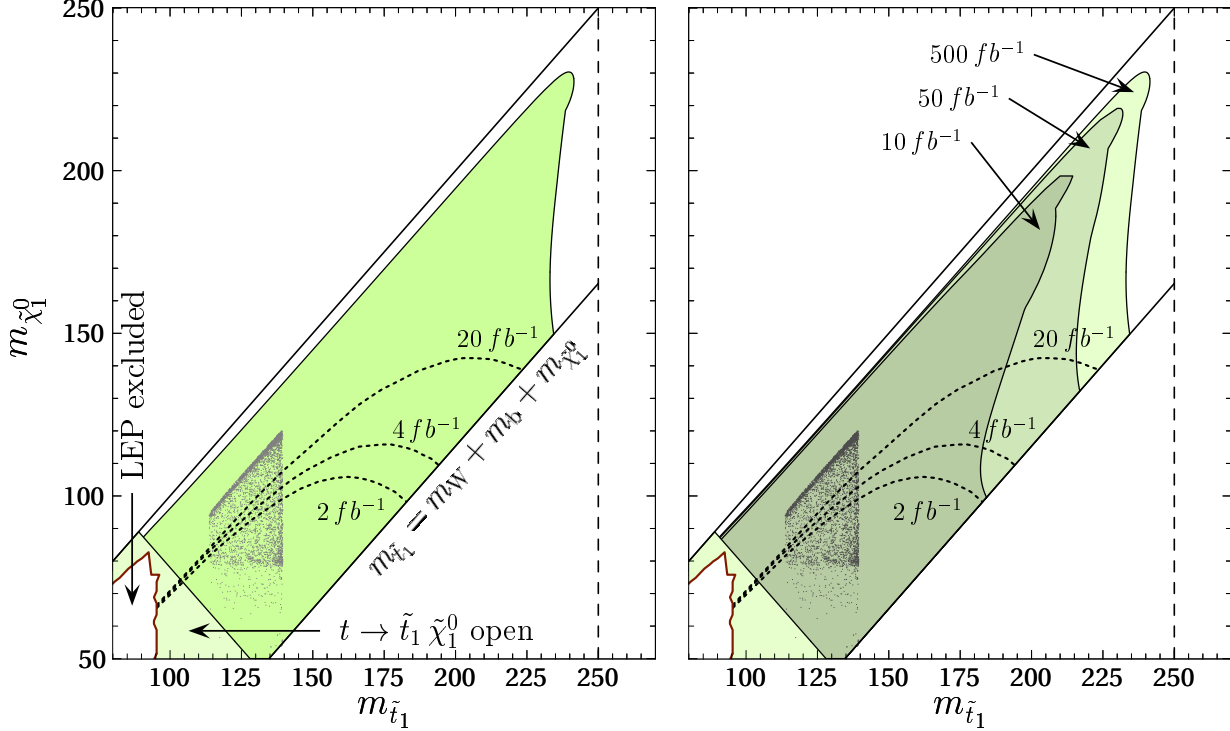


**Figure 1:** **Left:** Discovery reach of linear collider with  $500 \text{ fb}^{-1}$  luminosity and unpolarized beams at  $\sqrt{s} = 500 \text{ GeV}$  for production of light stops,  $e^+e^- \rightarrow \tilde{t}_1 \tilde{t}_1^* \rightarrow c\tilde{\chi}_1^0 \bar{c}\tilde{\chi}_1^0$ . The results are given in the stop vs. neutralino mass plane. In the dark shaded region, a  $5\sigma$  discovery is possible. The region where  $m_{\tilde{\chi}_1^0} > m_{\tilde{t}_1}$  is inconsistent with a neutralino LSP, while for  $m_{\tilde{t}_1} > m_W + m_b + \tilde{\chi}_1^0$  the three-body decay  $\tilde{t}_1 \rightarrow W^+ \bar{b} \tilde{\chi}_1^0$  becomes accessible and dominant. In the light shaded corner to the lower left, the decay of the top quark into a light stop and neutralino is open. The dark gray dots indicate the region consistent with baryogenesis and dark matter. Also shown are the parameter region excluded by LEP searches [13] (white area in lower left) and the projected Tevatron light stop reach [12] (dotted lines) for various integrated luminosities. **Right:** The same for different linear collider luminosities.

luminosity of  $10 \text{ fb}^{-1}$  is sufficient for this purpose. The results in Fig. 1 are given for unpolarized beams, but remain about the same if half of the luminosity is spent for left/right and right/left-polarized  $e^+/e^-$  beams, respectively. For an integrated luminosity of  $500 \text{ fb}^{-1}$ , the reach extends to stop masses  $m_{\tilde{t}_1}$  up to almost the beam energy  $\sqrt{s}/2 = 250 \text{ GeV}$ . In the plot, there is a dip in the covered region at roughly  $m_{\tilde{t}_1} = 240 \text{ GeV}$  and  $m_{\tilde{\chi}_1^0} = 170 \text{ GeV}$ . This is a result of the cut for the invariant di-jet mass around the  $W$  boson mass (cut 6).

## 4 Parameter determination

The discovery of light scalar top quarks, in conjunction with a Standard-Model-like Higgs boson with a mass near  $120 \text{ GeV}$ , would be a strong indication that electroweak baryoge-

$P(e^-)/P(e^+)$	0/0	-80%/+60%	+80%/-60%
Residual background cross-section [fb]	11.7	20.4	4.3

**Table 4:** Residual background level after final event selection for different beam polarizations.

genesis is the mechanism for the generation of the baryon asymmetry. At the same time, supersymmetry could also explain the existence of dark matter in the universe, based on the co-annihilation mechanism. In order to confirm this exciting picture, the relevant supersymmetry parameters have to be measured accurately.

One needs to (i) determine that the light stop is mainly right-chiral to contribute appropriately to the electroweak phase transition while being in agreement with electroweak precision measurements, (ii) check that the masses and compositions of the gauge/Higgs superfield sector are compatible with the values required for the generation of the baryon asymmetry, and (iii) compute the dark matter annihilation cross-sections and the relic abundance so as to compare with cosmological observations. If stop-neutralino co-annihilation is relevant it is important to determine the stop-neutralino mass difference very precisely.

In this section, the experimental determination of the relevant parameters in the stop and neutralino/chargino sectors will be discussed. As a first step, the analysis is based on tree-level formulae. In general, however, radiative corrections can be important and introduce a dependence on parameters of other sectors of the supersymmetric theory. This will be studied in a forthcoming publication.

In the following, a specific MSSM parameter point will be considered, as defined in the appendix. At tree-level the resulting neutralino and stop masses and mixing angle are:

$$m_{\tilde{t}_1} = 122.5 \text{ GeV}, \quad m_{\tilde{t}_2} = 4203 \text{ GeV}, \quad \cos \theta_{\tilde{t}} = 0.0105, \quad m_{\tilde{\chi}_1^0} = 107.2 \text{ GeV}. \quad (16)$$

Note that the stop mixing angle in this scenario is very small, resulting in an almost completely right-chiral light stop state. The mass difference  $\Delta m = m_{\tilde{t}_1} - m_{\tilde{\chi}_1^0} = 15.2 \text{ GeV}$  lies well within the sensitivity range of the linear collider.

## 4.1 Stop quark parameters

From the measurement of  $\tilde{t}_1 \tilde{t}_1^*$  production cross-section for different beam polarization combinations, both the mass of the light stop and the stop mixing angle can be extracted [41]. Here it is assumed that  $250 \text{ fb}^{-1}$  are spent for  $P(e^-)/P(e^+) = -80\%/+60\%$  and  $+80\%/-60\%$ , respectively, where negative polarization degrees indicate left-handed polarization and positive values correspond to right-handed polarization. Typical values for the stop production cross-sections for these beam polarizations are given in Table 1. The remaining background is summarized in Table 4. With these numbers, the cross-sections and statistical errors in the scenario defined in the appendix are  $\sigma[-80\%/+60\%] = (72 \pm 1.6) \text{ fb}$  and  $\sigma[+80\%/-60\%] = (276 \pm 2.2) \text{ fb}$ .<sup>5</sup> Besides the statistical error, the following systematic errors for the cross-section measurement are included:

<sup>5</sup>The cross-section values given here differ from Table 1 due to the different stop mixing angle.

- The mass of the lightest neutralino can be measured very precisely from the electron decay energy spectrum of the R-selectron, if the R-selectron is light enough to be produced in pairs at the linear collider. As described in detail in the next subsection, a precision of  $\delta m_{\tilde{\chi}_1^0} = 0.1$  GeV can be achieved with this method. The impact on the cross-section measurements is about 0.1%.
- It is assumed that the beam polarization degree can be determined with an uncertainty of  $\delta P(e^\pm)/P(e^\pm) = 0.5\%$ , which is a conservative estimate [42]. The effect of the polarization uncertainty on the stop cross-section determination is below 0.01%.
- In order to extract total cross-sections, the delivered luminosity needs to be determined, which can be measured quite accurately. According to Ref. [43], a precision of  $\delta\mathcal{L}/\mathcal{L} = 2 \times 10^{-4}$  seems feasible, but for this work a more conservative value of  $\delta\mathcal{L}/\mathcal{L} = 5 \times 10^{-4}$  is assumed.
- For the theoretical simulation of the Standard Model background  $B$ , a relative error of  $\delta B/B = 0.3\%$  is assigned. This estimate is based on the  $We\nu$  process as the largest background. While a complete NLO calculation of that process is still missing, a recent result for the related process of  $W$  pair production [44] suggests that a NLO calculation of  $We\nu$  is feasible within the next years with a remaining error well below 0.5%.
- Since the decay  $\tilde{t}_1 \rightarrow c\tilde{\chi}_1^0$  is loop-suppressed, the expected decay width is below 1 keV and the stop will hadronize before decay. The formation of the stop hadron and the fragmentation function of stop production cannot be predicted reliably today, leading to large errors in the stop searches at LEP [13]. However, if the stop is discovered at the linear collider, the uncertainties in the hadronization and fragmentation models can be reduced substantially by using experimental data [45]. Therefore the impact of this error on the cross-section determination is estimated to be at most 1%.
- The jet analysis and the charm tagging depends on the charm fragmentation function. Information about charm tagging can be gained at the linear collider itself from large samples of charm jets from Standard Model processes, such as  $Z \rightarrow c\bar{c}$ . Thus the remaining error should be small, below 0.5%.
- The realistic simulation of detector effects on the selection efficiency is limited by Monte-Carlo statistics and detector calibration. With the progress of future computing resources, the error stemming from Monte-Carlo statistics should be negligible. On the other hand, experience from LEP2 shows that the calibration uncertainty can be kept below 0.5% and should further improve with future detector research and development.
- For the computation of the cross-sections, beamstrahlung effects need to be understood precisely. The beamstrahlung spectrum can be extracted from Bhabha scattering with good accuracy [46]. The resulting error on the stop cross-section is found to be about 0.02%.

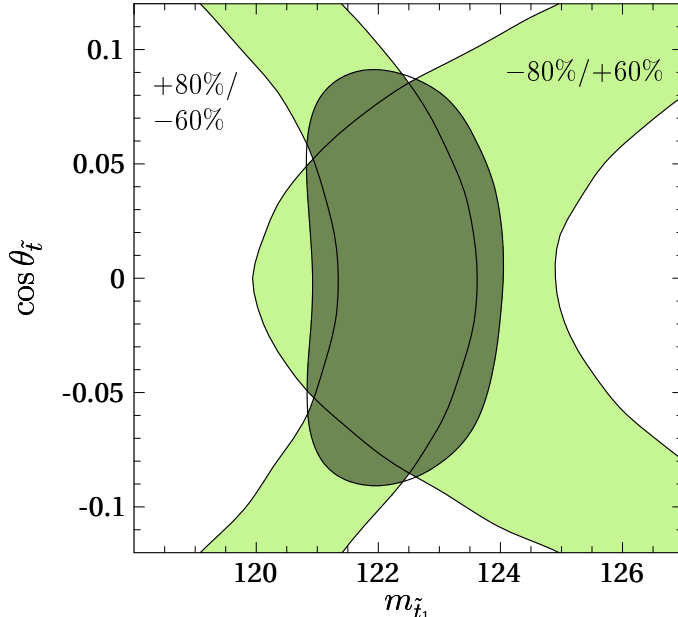


**Figure 2:** Determination of light stop mass  $m_{\tilde{t}_1}$  and stop mixing angle  $\theta_{\tilde{t}}$  from measurements of the cross-section  $\sigma(e^+e^- \rightarrow \tilde{t}_1\tilde{t}_1^*)$  for beam polarizations  $P(e^-)/P(e^+) = -80\%/+60\%$  and  $+80\%/-60\%$ . The widths of the light shaded bands indicate the  $1\sigma$  errors of the cross-section measurements, which are combined into the  $1\sigma$  two-parameter allowed region (dark shaded). The plot includes statistical and systematic errors.

- Finally, higher-order radiative corrections to the stop cross-section need to be under control. While no radiative corrections are included in this study, it is assumed that the relevant radiative corrections will be available at the time of start-up of the ILC, leaving a negligible theoretical error.

Adding up the individual error source in quadrature leads to a total systematic error of 1.3% for  $P(e^-)/P(e^+) = -80\%/+60\%$  polarization and 1.2% for  $+80\%/-60\%$  polarization, respectively. However, the above error estimate is rather conservative, giving the maximum expected error. Experience from many analyses at LEP and other colliders implies that data-driven systematics can be reduced to the level of the statistical error. This would in particular apply to the error from hadronization, fragmentation and detector calibration. Since all other systematic error sources are small, the total systematic error under this assumption is about the same as the statistical error of the collected signal events, *i.e.* about 0.8%. Combining statistical and systematic uncertainties, the total error for the cross-section determination amounts to 1.1% for  $P(e^-)/P(e^+) = -80\%/+60\%$  polarization and 2.4% for  $+80\%/-60\%$  polarization, respectively.

Each of the two cross-section measurements for  $P(e^-)/P(e^+) = -80\%/+60\%$  and  $+80\%/-60\%$  results in a band in the parameter plane of the stop mass and mixing angle, see Fig. 2. The widths of the bands reflects the uncertainty from statistical and systematic errors. Combining the two cross-section measurements, the resulting precision for the stop

parameter extraction is

$$m_{\tilde{t}_1} = (122.5 \pm 1.0) \text{ GeV}, \quad |\cos \theta_{\tilde{t}}| < 0.074 \quad \Rightarrow \quad |\sin \theta_{\tilde{t}}| > 0.9972. \quad (17)$$

As the stop mixing angle in this scenario is very small,  $\cos \theta_{\tilde{t}} = 0.0105$ , it cannot be experimentally distinguished from the zero mixing case. However, a strong upper bound on the mixing angle can be derived from the measurement.

## 4.2 Chargino and neutralino parameters

In Ref. [18,47], a general strategy for extracting the chargino and neutralino parameters is described. It relies on cross-section measurements of chargino and neutralino pair production at the linear collider and mass chargino and neutralino mass measurements from the linear collider and LHC. The mass determination of neutralinos and charginos at the LHC makes use of kinematical edges in the invariant mass spectra of the decay products of squark chains [48]. However, in the scenario under study here most of the squark states are assumed to be heavy to avoid the present electric dipole moment constraints [28]. The only light state is the light stop, which is predominantly right-chiral and directly decays to the bino LSP. As a consequence, the rate of chargino and neutralino production from squark cascades in this scenario is very small. In principle, charginos and neutralinos can also be produced directly through s-channel  $Z$ -boson and photon exchange, but the rates for these processes are also relatively small [49], rendering a reliable mass measurement impossible.

This analysis therefore has to be restricted to linear collider measurements. The following observables are included for extracting the fundamental gaugino/higgsino MSSM parameters:

- Chargino and neutralino mass measurements.
- Cross-section for pair production of the light chargino.
- Production cross-sections for the lightest and next-to-lightest neutralinos.

This study is restricted to the framework of the MSSM, assuming two chargino and four neutralino states with the free parameters  $M_1$ ,  $M_2$ ,  $\mu$  and  $\tan \beta$ . For the sample scenario in the appendix, the chargino and neutralino masses at tree-level amount to

$$\begin{aligned} m_{\tilde{\chi}_1^0} &= 107.2 \text{ GeV}, & m_{\tilde{\chi}_2^0} &= 196.1 \text{ GeV}, & m_{\tilde{\chi}_1^\pm} &= 194.3 \text{ GeV}, \\ m_{\tilde{\chi}_3^0} &= 325.0 \text{ GeV}, & m_{\tilde{\chi}_4^0} &= 359.3 \text{ GeV}, & m_{\tilde{\chi}_2^\pm} &= 358.1 \text{ GeV}. \end{aligned} \quad (18)$$

Furthermore, the scenario has been chosen such that the lighter, predominantly right-chiral, selectron state is accessible at the linear collider,  $m_{\tilde{e}_1} = 204.2 \text{ GeV}$ , while the other selectron and sneutrino states are heavy,  $m_{\tilde{e}_2}, m_{\tilde{\nu}_e} = 2 \text{ TeV}$ .

In this case, the mass of the lightest neutralino can be determined very precisely from the electron energy spectrum in selectron decay,  $\tilde{e}_1^\pm \rightarrow e^\pm \tilde{\chi}_1^0$ . Since the selectron is a scalar particle, the decay electron energy is to first approximation uniformly distributed between



the minimum and maximum value  $E_{\min}$  and  $E_{\max}$ , with the distribution edges being related to the selectron and neutralino masses,

$$E_{\min,\max} = \frac{\sqrt{s}}{4} \frac{m_{\tilde{e}_1}^2 - m_{\tilde{\chi}_1^0}^2}{m_{\tilde{e}_1}^2} \left( 1 \pm \sqrt{1 - 4m_{\tilde{e}_1}^2/s} \right). \quad (19)$$

In Ref. [51], this has been simulated in detail for the Snowmass parameter point SPS1a. The expected error for the determination of the spectrum edges can be extrapolated from that study by scaling the error with the differential cross-section. This is based on the observation that the total error is dominated by statistics, which under the assumption of Poisson statistics scales with the square root of the differential cross-section. The masses can then be derived from the measured values for the edge locations  $E_{\min,\max}$  using eq. (19), leading to

$$m_{\tilde{e}_1} = 204.2 \pm 0.09 \text{ GeV}, \quad m_{\tilde{\chi}_1^0} = 133.4 \pm 0.16 \text{ GeV}. \quad (20)$$

The extracted values for  $m_{\tilde{e}_1}$  and  $m_{\tilde{\chi}_1^0}$  are strongly correlated. Thus the precision can be further improved by using an independent measurement of the selectron mass from a  $e^-e^-$  threshold scan [35,50]. From the threshold scan with a total luminosity of  $5 \text{ fb}^{-1}$ , a precision of 85 MeV for the selectron mass is expected, leading in combination with eq. (20) to

$$m_{\tilde{\chi}_1^0} = 133.4 \pm 0.13 \text{ GeV}. \quad (21)$$

By including other channels, *i.e.* smuon decay spectra, the neutralino mass error can be further reduced to

$$m_{\tilde{\chi}_1^0} = 133.4 \pm 0.11 \text{ GeV}. \quad (22)$$

The most precise method for the determination of the other neutralino and chargino masses at a linear collider is from threshold scans. This has been studied in experimental simulations for the Snowmass parameter point SPS1a in Ref. [52]. A simple estimate of the expected error in the scenario defined in the appendix can be achieved by rescaling the results of Ref. [52] with the different cross-sections near threshold. Since the mass measurement error is dominated by statistics, the error should scale with the square root of the cross-section near threshold, assuming Poisson statistics. It is assumed that for each threshold scan an integrated luminosity of  $100 \text{ fb}^{-1}$  is invested, corresponding to a running time of a few months.

In the SPS1a scenario, the dominant decay mode of the chargino is into a tau lepton, neutrino and neutralino,  $\tilde{\chi}_1^\pm \rightarrow \tau^\pm \nu_\tau \tilde{\chi}_1^0$ . In the stop co-annihilation scenario, the chargino decays into the light stop,  $\tilde{\chi}_1^\pm \rightarrow \tilde{t}_1 \bar{b}$ , is also open. For the scenario under study, the branching ratio is  $\text{BR}(\tilde{\chi}_1^+ \rightarrow \tilde{t}_1 \bar{b}) = 98\%$ .

Since the stop decay is thus the dominant decay mode, the chargino pair production signal is characterized by two b-quark jets and two c-quark jets and missing energy originating from the neutralinos in the decay cascade,  $e^+e^- \rightarrow \tilde{\chi}_1^+ \tilde{\chi}_1^- \rightarrow \tilde{t}_1 \bar{b} \tilde{t}_1^* b \rightarrow c \tilde{\chi}_1^{0\bar{b}} \bar{c} \tilde{\chi}_1^{0b}$ . While a detailed experimental simulation for this channel is not available, we estimate the expected signal efficiency using results of other studies. The signal identification relies heavily on flavor identification. Demanding a purity of about 80% each, tagging efficiencies of about 80% and

40% for b-quark and c-quark pairs, respectively, are achievable [53]. The main backgrounds are triple gauge boson production, which is small [54], and  $t\bar{t}$  events. Both can be reduced by applying simple cuts on the di-jet invariant masses and the  $t\bar{t}$  background is strongly diminished by demanding large missing energy and an isolated lepton veto. Thus a resulting signal efficiency of 30% seems feasible, which is comparable with the efficiency for the decay of the charginos into taus in the SPS1a scenario [52]. Therefore the expected precision for the chargino mass measurements from a threshold scan can be estimated from the results of Ref. [52] by simply factoring in the different cross-section.

The main decay mode for the neutralino  $\tilde{\chi}_2^0$  in the scenario in the appendix is the leptonic decay  $\tilde{\chi}_2^0 \rightarrow l^+l^- \tilde{\chi}_1^0$ ,  $l = e, \mu, \tau$ , as in the SPS1a scenario. Therefore the background reduction is expected to be similar as described in Ref. [52] and a comparable resulting experimental efficiency can be assumed. The main difference to be taken into account is therefore again the value of the production cross-section  $e^+e^- \rightarrow \tilde{\chi}_1^0\tilde{\chi}_2^0$  near threshold.

For the heavier neutralino states, no detailed simulations exist so far. Preliminary studies [55] suggest that if the decay channels into gauge bosons,  $\tilde{\chi}_{3,4}^0 \rightarrow Z\tilde{\chi}_i^0, W^\pm\tilde{\chi}_1^\mp$ , are dominant, the neutralino mass can be reconstructed from their decay spectra with a precision of 3–5 GeV. Here an error of 4 GeV is assumed for the mass of  $\tilde{\chi}_3^0$ , which is produced in  $e^+e^- \rightarrow \tilde{\chi}_1^0\tilde{\chi}_3^0$ . The neutralino  $\tilde{\chi}_4^0$  and the heavier chargino  $\tilde{\chi}_2^\pm$  are too heavy to be studied at a 500 GeV collider.

Under these assumption the following error estimates are obtained:

$$\delta m_{\tilde{\chi}_1^0} = 0.11 \text{ GeV}, \quad \delta m_{\tilde{\chi}_2^0} = 2.5 \text{ GeV}, \quad \delta m_{\tilde{\chi}_3^0} \approx 4 \text{ GeV}, \quad \delta m_{\tilde{\chi}_1^\pm} = 0.12 \text{ GeV}. \quad (23)$$

Note that the precision for the chargino mass is substantially better than in Ref. [52], where  $\delta m_{\tilde{\chi}_1^\pm} = 0.55 \text{ GeV}$  was obtained. This can be explained by the fact that for the SPS1a scenario there is a large cancellation between the s- and t-channel contributions to chargino production. In the scenario defined in the appendix, on the other hand, the t-channel is suppressed due to the large sneutrino mass, so that the cancellation does not occur and the cross-section is about 20 times larger.

The mass measurements are not sufficient to extract the fundamental supersymmetry parameters without ambiguity. Additional information is obtained from measurements of the chargino and neutralino cross-sections. The chargino cross-section is relatively large, about 1 pb, depending on the beam polarization, and gives important information through the chargino couplings and mixings. Using the possibility of beam polarization, two independent cross-section measurements with left/right- and right/left-polarized  $e^-/e^+$  beams can be performed at  $\sqrt{s} = 500 \text{ GeV}$ ,  $\sigma_L^{\tilde{\chi}_1^+\tilde{\chi}_1^-}(500)$  and  $\sigma_R^{\tilde{\chi}_1^+\tilde{\chi}_1^-}(500)$ .

As discussed above, the chargino decays dominantly into the light stop,  $\tilde{\chi}_1^+ \rightarrow \tilde{t}_1 \bar{b}$ . As the branching ratios are difficult to determine experimentally, here only the larger chargino decay channel  $\tilde{\chi}_1^+ \rightarrow \tilde{t}_1 \bar{b}$  will be considered, and for the parameter extraction only cross-section ratios, not absolute cross-sections, are used. Besides the ratio of the cross-section for different beam polarizations,  $\sigma_L^{\tilde{\chi}_1^+\tilde{\chi}_1^-}(500)/\sigma_R^{\tilde{\chi}_1^+\tilde{\chi}_1^-}(500)$ , ratios of the cross-section at other center-of-mass energies do not yield any significant additional information in the scenario in the appendix. This can be understood by the fact that the dependence of the cross-section

on the center-of-mass energy is small since the t-channel contributions is switched off due to the large sneutrino mass.

For the measurement of  $\sigma_{\text{L}}^{\tilde{\chi}_1^+ \tilde{\chi}_1^-}$  (500) and  $\sigma_{\text{R}}^{\tilde{\chi}_1^+ \tilde{\chi}_1^-}$  (500), a luminosity of  $250 \text{ fb}^{-1}$  each is assumed. As before, 80%  $e^-$  and 60%  $e^+$  beam polarization are used. As discussed above, due to relatively small backgrounds, it is estimated that an overall signal efficiency of 30% can be achieved for the chargino decay mode into stops. Systematic errors mainly arise from the following sources:

- The error on the chargino mass  $\delta m_{\tilde{\chi}_1^\pm} = 0.12 \text{ GeV}$  from a threshold scan [52].
- The error on the electron-sneutrino mass  $m_{\tilde{\nu}_e}$ , which enters into the production process through the t-channel exchange contribution. Since the sneutrino is heavy, only a lower bound on the mass can be set, which is assumed to be  $m_{\tilde{\nu}_e} > 1000 \text{ GeV}$ .
- As above, an uncertainty of  $\delta P(e^\pm)/P(e^\pm) = 0.5\%$  is assigned for the beam polarization [42].

The cross-section ratio and the two chargino masses are related to the fundamental parameters  $M_2$ ,  $|\mu|$ ,  $\phi_\mu$  and  $\tan \beta$  by eqs. (5) and the formulae in Ref. [18].

Evidently, three observables are not sufficient to extract these four parameters. In addition, the heavy chargino  $\tilde{\chi}_2^\pm$  is difficult to access at the linear collider, while the identification of charginos at the LHC is difficult because the hadronic chargino decay is faced with large backgrounds. Moreover, the chargino observables exhibit substantial correlations. For these reasons, and to constrain the missing parameter  $M_1$ , also neutralino observables are included in the analysis.

Neutralinos can be produced in various pair combinations,  $e^+e^- \rightarrow \tilde{\chi}_i^0 \tilde{\chi}_j^0$ ,  $i, j = 1 \dots 4$ . However, the production rates for  $\tilde{\chi}_3^0$  and  $\tilde{\chi}_4^0$  are small and the heavy states decay via complex cascades. Therefore, here only the production cross-sections of the two lighter states are considered,  $e^+e^- \rightarrow \tilde{\chi}_1^0 \tilde{\chi}_2^0$  and  $e^+e^- \rightarrow \tilde{\chi}_2^0 \tilde{\chi}_2^0$ . In contrast to the charginos, the  $\tilde{\chi}_2^0$  cannot decay into stop quarks, leaving only the leptonic decay modes open. This allows to measure absolute cross-sections. For  $\sigma(e^+e^- \rightarrow \tilde{\chi}_1^0 \tilde{\chi}_2^0)$ , an experimental simulation was performed in Ref. [56], yielding an efficiency of 25% in SPS1a. For the process  $e^+e^- \rightarrow \tilde{\chi}_2^0 \tilde{\chi}_2^0$  no detailed simulation exists. It leads to a final state of four leptons (mainly taus for the case of large  $\tan \beta \gtrsim 5$ ) and two LSPs, which result in missing energy in the detector. This signature has very little background. From the tau tagging efficiency achieved in Ref. [56], it is expected that  $\sigma(e^+e^- \rightarrow \tilde{\chi}_2^0 \tilde{\chi}_2^0)$  can be reconstructed with an efficiency of 15%.

The two neutralino cross-sections  $\sigma(e^+e^- \rightarrow \tilde{\chi}_1^0 \tilde{\chi}_2^0)$  and  $\sigma(e^+e^- \rightarrow \tilde{\chi}_2^0 \tilde{\chi}_2^0)$  can be measured again for the two polarization combinations  $P(e^-)/P(e^+) = -80\%/+60\%$  and  $+80\%/-60\%$  at  $\sqrt{s} = 500 \text{ GeV}$ .

In total this amounts to four observables from the neutralino cross-sections. Systematic errors due to the uncertainty of the selectron masses in the t-channel contributions and of the beam polarization are taken into account. The expected precision for the light selectron mass is  $\delta m_{\tilde{e}_1} = 0.085 \text{ GeV}$  from a threshold scan, while for the heavy selectron mass only

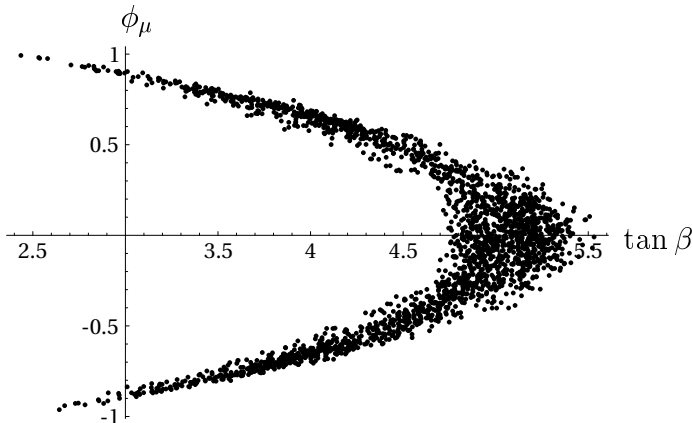


**Figure 3:** Allowed region in the  $\tan\beta$ - $\phi_\mu$  parameter plane from measurements in the chargino/neutralino sector. The black dots correspond to points from a random scan over all parameters that are allowed by the condition  $\Delta\chi^2 \leq 1$ .

a lower bound can be set, which is assumed to be  $m_{\tilde{e}_2} > 1000$  GeV. For the polarization uncertainty the same value  $\delta P(e^\pm)/P(e^\pm) = 0.5\%$  as above is taken.

The neutralino cross-sections and masses can be related to the parameters  $M_1$ ,  $M_2$ ,  $|\mu|$ ,  $\phi_\mu$  and  $\tan\beta$  using the formulae of Ref. [20]. The chargino and neutralino cross-section and mass measurements are combined in a  $\chi^2$  fit, thus taking into account all correlations. The fit results are

$$\begin{aligned}
 M_1 &= (112.6 \pm 0.2) \text{ GeV}, \\
 M_2 &= (225.0 \pm 0.7) \text{ GeV}, \\
 |\mu| &= (320.0 \pm 3.0) \text{ GeV}, \\
 |\phi_\mu| &< 1.0, \\
 \tan\beta &= 5_{-2.6}^{+0.5}.
 \end{aligned}
 \tag{24}$$

Due to correlations, the resulting  $1\sigma$  bounds on the fundamental MSSM parameter are not very precise for some of the parameters. In particular, for the given scenario defined in the appendix, there is a large correlation between  $\tan\beta$  and the CP-violation phase  $\phi_\mu$ , as shown in Fig. 3. As a consequence a precise determination of the two parameters individually is difficult from the chargino and neutralino sector alone. Ref. [57] suggests that  $\tan\beta$  can be determined accurately in the Higgs sector, but this has not been studied for the case of CP violation so far.

### 4.3 Higgs parameters

The s-channel Higgs resonances could be important for the dark matter annihilation cross-section, hence the Higgs parameters have to be determined independently. In the present scenario given in the appendix, the Higgs and neutralino masses are such that none of the Higgs states forms a resonance in the neutralino annihilation. The experimental verification of this scenario requires at least a rough measurement of the Higgs masses and couplings.

By studying the Higgs-strahlung process  $e^+e^- \rightarrow Zh^0$ , the mass of a light Higgs boson with  $m_H \approx 120$  GeV can be determined with an error of less than 100 MeV [58, 59] and the couplings of the Higgs to Standard Model fermions can be extracted with a precision of a few percent [59, 60]. The Higgs-neutralino coupling is difficult to measure, but it can be calculated from the fermionic couplings within the MSSM. In addition, a model-independent upper bound on the Higgs-neutralino coupling follows from requiring this coupling to be in the perturbative regime. This information on the Higgs mass and couplings is sufficient to verify that the impact of Higgs exchange on the annihilation process is completely negligible in the given scenario in the appendix, since the annihilation proceeds far away from the Higgs resonance.

The heavier Higgs states cannot be studied at a 500 GeV linear collider. However, from searches for the process  $e^+e^- \rightarrow h^0A^0$ , a lower bound on the pseudoscalar mass of about  $m_{A^0} \sim 380$  GeV can be established, which is sufficient to rule out a significant contribution from the heavy Higgs bosons to the annihilation cross-section.

## 5 Dark matter prediction

The experimental data from collider experiments discussed in the previous section can be used to compute the expected cosmological dark matter relic density from supersymmetric sources. The given sample scenario in the appendix lies in the region where neutralino-stop co-annihilation is effective. Therefore it is expected that a precise prediction will dominantly rely on the accurate determination of the stop-neutralino mass difference.

While most of the individual measurements are quite precise, large correlations are found in the extraction of the chargino/neutralino parameters, as discussed at the end of section 4.2. However, since the dark matter computation mainly depends on the LSP mass  $m_{\tilde{\chi}_1^0}$ , which is measured directly, the resulting uncertainty due to experimental errors in the chargino/neutralino sector is relatively small when taking into account the correlations properly.

The relic dark matter density is computed with the program described in Ref. [24] and has been checked against the code ISAReD presented in Ref. [61]. The relevant parameters used as input and derived from the experimental analyses are  $m_{\tilde{t}_1}$ ,  $\cos\theta_{\tilde{t}}$ ,  $M_1$ ,  $M_2$ ,  $|\mu|$ ,  $\phi_\mu$ ,  $\tan\beta$ ,  $\sin\alpha$  and  $m_{h^0}$ . The mass of the heavier stop  $\tilde{t}_2$  is too large to be measured directly, but it is assumed that a limit of  $m_{\tilde{t}_2} > 1000$  GeV can be set from collider searches. In principle all other MSSM parameters have some effect on the dark matter annihilation and should be taken into account, but for the given scenario in the appendix, their contribution is sub-dominant and even rough estimates or lower mass bounds will be sufficient for an accurate computation of  $\Omega_{\text{CDM}}$ . Therefore the influence of these other parameters has been neglected here.

The expected experimental errors are propagated and correlations are taken into account by means of a  $\chi^2$  analysis. No theoretical errors due to higher order contributions are taken into account in the calculation of the dark matter density. The result for the scenario given in the appendix is shown in Fig. 4. The scattered dots indicate a scan of 100000 random

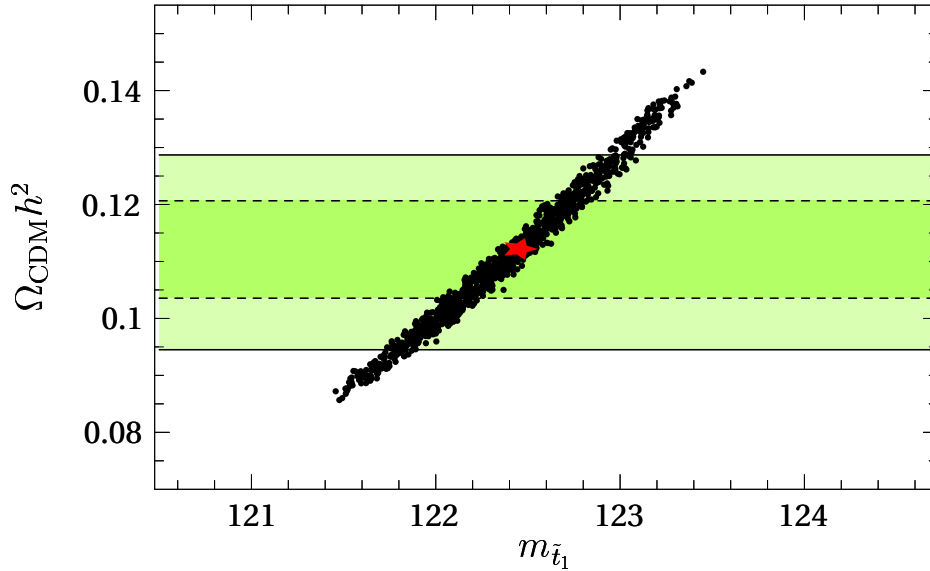


**Figure 4:** Computation of dark matter relic abundance  $\Omega_{\text{CDM}} h^2$  taking into account estimated experimental errors for stop, chargino, neutralino and Higgs sector measurements at future colliders. The black dots correspond to a scan over the  $1\sigma$  ( $\Delta\chi^2 \leq 1$ ) region allowed by the experimental errors, as a function of the measured stop mass, with the red star indicating the best-fit point. The horizontal shaded bands show the  $1\sigma$  and  $2\sigma$  constraints on the relic density measured by WMAP.

points in the parameter space allowed by the collider experimental results, as a function of the measured stop mass. The range of the horizontal axis is constrained by the error in the stop mass measurement,  $m_{\tilde{t}_1} = (122.5 \pm 1.0)$  GeV. The horizontal bands depict the relic density as measured by WMAP [1] with one and two standard deviation errors. At  $1\sigma$  level, the astrophysical observations lead to  $0.104 < \Omega_{\text{CDM}} h^2 < 0.121$ .

In total, using the collider measurements of the stop and chargino/neutralino as input to compute the dark matter annihilation cross-section, the relic density could be predicted to  $0.086 < \Omega_{\text{CDM}} h^2 < 0.143$  at the  $1\sigma$  level. Thus the overall precision is of the same magnitude as, but worse by roughly a factor 3 than the direct WMAP determination. The uncertainty in the theoretical determination is dominated by the measurement of the  $\tilde{t}_1$  mass.

The precision for the determination of the dark matter density from collider data could in principle be increased by including other stop mass measurements. Different methods for the  $\tilde{t}_1$  mass measurement have been analyzed in Ref. [62]. Besides using cross-section measurements with two beam polarization combinations, as detailed above,  $m_{\tilde{t}_1}$  can also be obtained from a scan near the  $\tilde{t}_1 \tilde{t}_1^*$  production threshold or from the charm jet energy distributions in the decay  $\tilde{t}_1 \rightarrow c \tilde{\chi}_1^0$ . In preliminary studies of these methods, accuracies of the order of 1–2 GeV were obtained [62], which does not improve on the stop mass measurement from the total production cross-section.

However, first results of an optimized threshold scan method indicate that the precision for  $m_{\tilde{t}_1}$  can be improved to about 0.5 GeV [63]. The advantage of the threshold scan method

	A	B	C	D	E	F
$m_{\tilde{U}_3}^2$ [GeV <sup>2</sup> ]	-99 <sup>2</sup>	-99 <sup>2</sup>	-99 <sup>2</sup>	-97 <sup>2</sup>	-90.5 <sup>2</sup>	-85.5 <sup>2</sup>
$m_{\tilde{Q}_3}$ [GeV]	2700	3700	4200	4900	4700	4300
$A_t$ [GeV]	-860	-1150	-1050	-500	-400	0
$M_1$ [GeV]	107.15	111.6	112.6	119.0	123.2	129.0
$\tan\beta$	5.2	4	5	6	5.5	5.5
$A_{e,\mu,\tau}$	$5 \times e^{i\pi/2}$	$3.7 \times e^{i\pi/2}$	$5 \times e^{i\pi/2}$	$5.8 \times e^{i\pi/2}$	$5.2 \times e^{i\pi/2}$	$5 \times e^{i\pi/2}$
$m_{\tilde{t}_1}$ [GeV]	117.1	118.0	122.5	130.2	135.2	139.4
$m_{\tilde{\chi}_1^0}$ [GeV]	102.1	104.1	107.2	114.0	118.1	123.1
$\cos\theta_{\tilde{t}}$	0.0210	0.0150	0.0105	0.0038	0.0035	0.0005
$m_{h^0}$ [GeV]	115.1	115.0	117.0	117.1	116.2	115.1
$\Omega_{\text{CDM}}h^2$	0.113	0.060	0.112	0.144	0.166	0.112

**Table 5:** A few exemplary supersymmetry scenarios that are compatible with electroweak baryogenesis and bounds on the Higgs mass and the electron electric dipole moment. All other parameters not in the table are as in eq. (25) in the appendix. The scenario C is identical with the scenario in the appendix.

is the small influence of systematic errors, since it makes use of the shape of the cross-section as a function of the center-of-mass energy, instead of absolute cross-section measurements. However it is limited by small statistics near the threshold. The best accuracy can be achieved by combining a measurement near the threshold, where the cross-section is most sensitive to the stop mass, with a measurement at higher energies, where the cross-section is larger [63].

With an stop mass error of  $\delta m_{\tilde{t}_1} = 0.5$  GeV, the relic density could be computed much more precisely, yielding the result  $0.099 < \Omega_{\text{CDM}}h^2 < 0.125$  in the scenario defined in the appendix. This precision is very comparable to the direct WMAP determination.

The sample scenario in the appendix represents just one particular possible supersymmetry parameter point that has been chosen to give the correct dark matter relic density. It is also interesting to explore other cases, with different values of the stop mass and where the dark matter abundance derived from collider measurements would not overlap with the value obtained from astrophysical experiments. Table 5 lists six examples of supersymmetry scenarios that differ mainly in the stop parameters and the stop-neutralino mass difference  $\Delta m = m_{\tilde{t}_1} - m_{\tilde{\chi}_1^0}$ . All points are in agreement with the baryogenesis conditions of a strongly first order electroweak phase transition,  $v(T_c)/T_c \gtrsim 1$ , and a sufficiently large baryon asymmetry,  $\eta \sim 0.6 \times 10^{-10}$ . The constraints from the bounds on the Higgs mass from LEP,  $m_{h^0} \gtrsim 114.4$  GeV, and on the electron electric dipole moment are also taken into account.

The points A, C and F give a dark matter density in good agreement with current astrophysical observations. Here the scenario C is identical with the one introduced in the appendix. The point D is marginally consistent with the WMAP constraints, while the

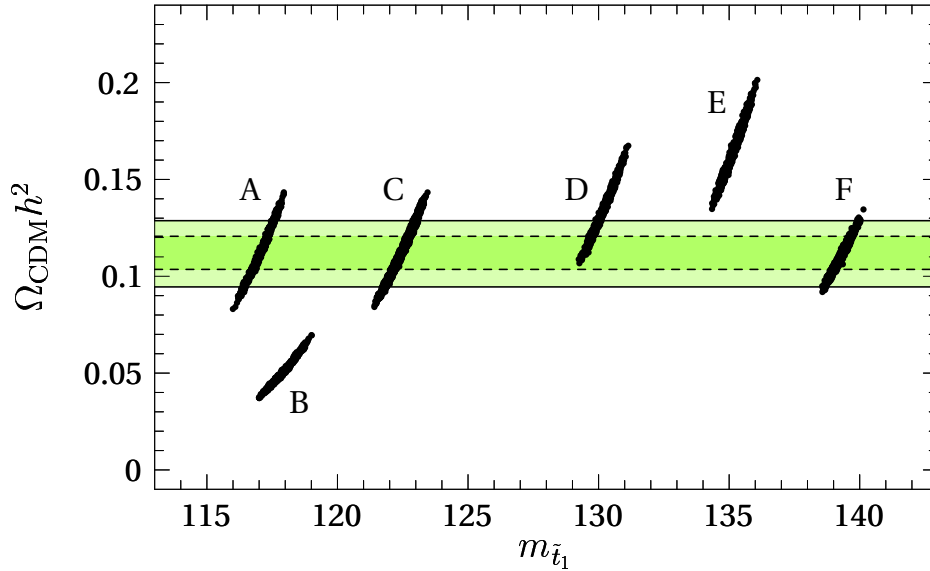


**Figure 5:** Supersymmetric dark matter relic abundance  $\Omega_{\text{CDM}}h^2$  predicted from collider stop, chargino, neutralino and Higgs sector measurements in different assumed supersymmetry scenarios from Table 5. The black dots correspond  $\chi^2$  scans over the supersymmetry parameter region allowed by projected  $1\sigma$  experimental errors. The horizontal shaded bands show the  $1\sigma$  and  $2\sigma$  constraints on the relic density measured by WMAP.

points B and E result in a dark matter density below and above, respectively, the WMAP measurement by more than the 95% confidence level.

Performing the analysis of experimental uncertainties as explained in the previous section for each of the points in Table 5 leads to the results shown in Fig 5. As evident from the figure, the linear collider measurements constrain the computed dark matter relic density with a precision comparable to the current direct astrophysical observation. For the points A, C and F this would indicate strong evidence that supersymmetry with a LSP neutralino and a light stop contributing to the co-annihilation mechanism is the source of dark matter in the universe.

In case of scenario D, the linear collider data would restrict the dark matter abundance to  $0.107 < \Omega_{\text{CDM}}h^2 < 0.167$  within  $1\sigma$  experimental errors. While this result would still be consistent with the current astrophysical result  $0.095 < \Omega_{\text{CDM}}h^2 < 0.129$  from WMAP, it imposes constraints on the supersymmetric parameter space. Under the assumption that our understanding of the cosmological evolution is correct, the  $\tilde{t}_1$  mass is for example required to be less than about 130 GeV.

For point E, the deduced neutralino dark matter density turns out to be too large compared to the WMAP result by roughly two standard deviations. This could be due to other particles contributing to increase the total dark matter annihilation cross-section. It can also be interpreted as evidence that our current theoretical understanding of the evolution of the universe needed to be revised. On the other hand, scenario B leads to a dark matter density that is smaller than the WMAP result by about two standard deviations. This discrepancy



could be explained by the existence of another source for cold dark matter or, as before, might put our description of cosmological evolution into question.

## 6 Conclusions and outlook

The MSSM with light scalar top quarks provides a framework for simultaneously explaining electroweak baryogenesis and the correct dark matter relic density. The stop-neutralino co-annihilation mechanism can play an important part in this picture. The exploration of this scenario relies on precision measurements at accelerator experiments and will be within reach for the next generation of colliders, in particular the ILC.

Based on a detailed experimental simulation including detector effects, it was shown that light stop quarks can be discovered at the ILC for stop masses up to almost the beam energy and for stop-neutralino mass differences  $\Delta m = m_{\tilde{t}_1} - m_{\tilde{\chi}_1^0}$  down to about 5 GeV. In particular, the complete parameter region where stop-neutralino co-annihilation is effective can be covered. Since stops with small  $\Delta m$  are difficult to explore at hadron colliders, the ILC thus provides a unique discovery capability for this kind of scenario.

In addition, it was found that the stop mass and mixing angle can be accurately determined from measurements of the stop production cross-section for two different beam polarizations at the ILC. Together with precision measurements in the chargino and neutralino sector, this would allow to compute the dark matter relic density from experimental results at the ILC in a bottom-up approach, *i.e.* without assuming a specific mechanism or pattern for supersymmetry breaking parameters. Including statistical and systematic errors in the experimental analysis, it was estimated that the precision for the relic density induced from ILC measurements is slightly worse, but comparable with the current direct determination from WMAP and SDSS. Refinements in the determination of the stop mass can improve this result significantly.

In MSSM scenarios that are consistent with electroweak baryogenesis, the lower limit on the Higgs boson mass from searches at LEP and bounds from electric dipole moments, the sfermions of the first two generations need to be relatively heavy. As a consequence, for these scenarios the exploration of supersymmetric partners and their properties is difficult at the LHC. Nevertheless, the LHC can establish lower limits on the masses of heavy superpartners, thus providing important information for the understanding and computation of the dark matter density in the universe.

The present scenario with light scalar top quark and small stop-neutralino mass differences is also a motivation for refining the development of the vertex detector. The analysis is based on a fast and realistic simulation of a detector which includes a CCD vertex tracker. The importance of the vertex detector performance for c-quark tagging in scalar top quark decays has been discussed in the framework of the Linear Collider Flavour Identification (LCFI) collaboration which studies CCD detectors for quark flavour identification. Regarding the vertex detector design, the study of c-quark tagging with small visible energy, as expected from the scalar top decays in the discussed scenario, is particularly challenging and could serve well as a benchmark reaction.

This paper is the first step in a larger project aiming to explore in detail the collider signatures and measurements that can elucidate the origin of baryonic and dark matter in the universe within the framework of supersymmetry. Future avenues include refinements in the experimental analysis, especially for small mass differences  $\Delta m$ , and the investigation of the impact of the vertex detector layout on the charm tagging performance.

In this work, the experimental analysis was designed with a selection procedure that is independent of the actual values of the unknown supersymmetry parameters. Such a search strategy, which does not require any prior knowledge of the supersymmetry scenario, is important for a model-independent discovery potential. However, once evidence for a stop signal would be found and the stop and neutralino mass would be measured with some precision, the analysis can be refined using this knowledge, in order to achieve a better separation of signal and background and increase the precision of the stop parameter determination.

In the present analysis, the projected uncertainty in the computation of the dark matter abundance is dominated by the error in the stop mass. By including other methods for the stop mass measurement, the precision for the dark matter computation could possibly be improved substantially. A promising possibility is a method making use of cross-section measurements near the pair production threshold, which seems to be able to reduce the stop mass error by a factor of two.

The present work has been performed using tree-level formulae and cross-sections for the ILC analysis and the computation of the dark matter annihilation rate. For the expected experimental precision, however, radiative corrections are important and introduce a dependence on other supersymmetry parameters, *e.g.* sfermion masses and mixing outside of the stop sector. This issue will be studied in future work.

In this publication a specific MSSM scenario was studied in detail for the experimental determination of parameters and the dark matter analysis. In future work, this analysis shall be extended to other scenarios that are similarly cosmologically motivated, but have different collider signatures.

The study presented in this report opens a window toward exploring some of the main unsolved questions in the evolution of the universe by establishing cross-relations between collider measurements and cosmological processes and by combining experimental analyses and theoretical computations. A sophisticated phenomenological program with precision measurements of new physics properties at the ILC sets the base for deepening our understanding of the cosmos.

## Appendix: MSSM case study scenario

The numerical analysis in sections 4 and 5 are based on a specific MSSM parameter point characterized by the following values:

$$\begin{aligned}
 m_{\tilde{U}_3}^2 &= -99^2 \text{ GeV}^2, & M_1 &= 112.6 \text{ GeV}, \\
 m_{\tilde{Q}_3} &= 4200 \text{ GeV}, & M_2 &= 225 \text{ GeV}, \\
 m_{\tilde{D}_3} &= 4000 \text{ GeV}, & |\mu| &= 320 \text{ GeV}, \\
 A_t &= -1050 \text{ GeV}, & \phi_\mu &= 0.2, \\
 m_{\tilde{L}_{1,2,3}} &= 2000 \text{ GeV}, & \tan \beta &= 5, \\
 m_{\tilde{R}_{1,2,3}} &= 200 \text{ GeV}, & m_{A^0} &= 800 \text{ GeV}, \\
 A_{e,\mu,\tau} &= 5 \text{ TeV} \times e^{i\pi/2}, \\
 m_{\tilde{Q},\tilde{U},\tilde{D}_{1,2}} &= 4000 \text{ GeV}.
 \end{aligned} \tag{25}$$

The potentially large contribution of one-loop sfermion-neutralino and sfermion-chargino loops to the electric dipole moments of the electron and neutron requires the sleptons and squarks of the first two generations to be heavy. Therefore all squark soft supersymmetry breaking parameters of the first two generations are taken to be 4 TeV, and in addition, the left-chiral sleptons are also assumed to be heavy. The right-chiral sleptons contribute to the electron electric dipole moment on a sub-leading level and can be taken with a mass of a few hundred GeV if the selectron  $A$ -parameter carries a CP-violating phase that cancels part of the effect of the phase of  $\mu$ . Here, the right-chiral slepton soft supersymmetry breaking mass is assumed to be 200 GeV, resulting in physical R-slepton masses within the kinematical reach of a 500 GeV linear collider.

The chosen parameters are compatible with a strongly first order electroweak phase transition for electroweak baryogenesis,  $v(T_c)/T_c \gtrsim 1$  [7], generate a sufficiently large baryon asymmetry,  $\eta \sim 0.6 \times 10^{-10}$ , and yield a value for the dark matter relic abundance<sup>6</sup> within the WMAP bounds,  $\Omega_{\text{CDM}} h^2 = 0.1122$ . In addition, the supersymmetry parameters, in particular the stop parameters, are chosen such that the mass of the lightest Higgs boson is  $m_{h^0} = 117 \text{ GeV}$ , sufficiently above the bound from direct searches at LEP  $m_{h^0} \gtrsim 114.4 \text{ GeV}$  [21]. At tree-level the following masses are obtained for the relevant supersymmetric particles:

$$\begin{aligned}
 m_{\tilde{t}_1} &= 122.5 \text{ GeV}, & m_{\tilde{e}_1} &= 204.2 \text{ GeV}, & m_{\tilde{\chi}_1^0} &= 107.2 \text{ GeV}, & m_{\tilde{\chi}_1^\pm} &= 194.3 \text{ GeV}, \\
 m_{\tilde{t}_2} &= 4203 \text{ GeV}, & m_{\tilde{e}_2} &= 2 \text{ TeV}, & m_{\tilde{\chi}_2^0} &= 196.1 \text{ GeV}, & m_{\tilde{\chi}_2^\pm} &= 358.1 \text{ GeV}, \\
 \cos \theta_{\tilde{t}} &= 0.0105, & m_{\tilde{\nu}_e} &= 2 \text{ TeV}, & m_{\tilde{\chi}_3^0} &= 325.0 \text{ GeV}, \\
 & & & & m_{\tilde{\chi}_4^0} &= 359.3 \text{ GeV}.
 \end{aligned} \tag{26}$$

---

<sup>6</sup>The relic dark matter density has been computed with the code used in Ref. [24].

## Acknowledgments

The authors greatly benefited from practical advice by S. Mrenna about PYTHIA, by P. Bechtel about SIMDET and by T. Kuhl about the c-tagging procedure. Special thanks go to C. Balázs for useful discussions and assistance with the program ISAReD, and to M. Schmitt for proofreading of the manuscript and very valuable comments.

## References

- [1] D. N. Spergel *et al.* [WMAP Collaboration], *Astrophys. J. Suppl.* **148**, 175 (2003).
- [2] M. Tegmark *et al.* [SDSS Collaboration], *Phys. Rev. D* **69**, 103501 (2004).
- [3] A. D. Sakharov, *Pisma Zh. Eksp. Teor. Fiz.* **5**, 32 (1967) [*JETP Lett.* **5**, 24 (1967) SOPUA,34,392-393.1991 UFNAA,161,61-64.1991].
- [4] A. I. Bochkarev and M. E. Shaposhnikov, *Mod. Phys. Lett. A* **2**, 417 (1987).
- [5] K. Kajantie, M. Laine, K. Rummukainen and M. E. Shaposhnikov, *Phys. Rev. Lett.* **77**, 2887 (1996)
- [6] G. R. Farrar and M. E. Shaposhnikov, *Phys. Rev. Lett.* **70**, 2833 (1993) [Erratum-ibid. **71**, 210 (1993)];  
G. R. Farrar and M. E. Shaposhnikov, *Phys. Rev. D* **50**, 774 (1994);  
M. B. Gavela, P. Hernandez, J. Orloff, O. Pène and C. Quimbay, *Nucl. Phys. B* **430**, 382 (1994).
- [7] M. Carena, M. Quirós and C. E. M. Wagner, *Phys. Lett. B* **380**, 81 (1996).
- [8] M. Laine, *Nucl. Phys. B* **481**, 43 (1996) [Erratum-ibid. B **548**, 637 (1999)];  
M. Losada, *Phys. Rev. D* **56**, 2893 (1997);  
G. R. Farrar and M. Losada, *Phys. Lett. B* **406**, 60 (1997);  
B. de Carlos and J. R. Espinosa, *Nucl. Phys. B* **503**, 24 (1997);  
D. Bodeker, P. John, M. Laine and M. G. Schmidt, *Nucl. Phys. B* **497**, 387 (1997).
- [9] M. Carena, M. Quirós and C. E. M. Wagner, *Nucl. Phys. B* **524**, 3 (1998).
- [10] M. Laine and K. Rummukainen, *Nucl. Phys. B* **535**, 423 (1998);  
M. Losada, *Nucl. Phys. B* **537**, 3 (1999);  
M. Losada, *Nucl. Phys. B* **569**, 125 (2000);  
M. Laine and M. Losada, *Nucl. Phys. B* **582**, 277 (2000);  
M. Laine and K. Rummukainen, *Nucl. Phys. B* **597**, 23 (2001).
- [11] C. Balázs, M. Carena and C. E. M. Wagner, *Phys. Rev. D* **70**, 015007 (2004).

- [12] R. Demina, J. D. Lykken, K. T. Matchev and A. Nomerotski, *Phys. Rev. D* **62**, 035011 (2000).
- [13] LEP2 SUSY Working Group, ALEPH, DELPHI, L3 and OPAL experiments, note LEPSUSYWG/04-02.1 [<http://lepsusy.web.cern.ch/lepsusy/>].
- [14] H. Murayama and A. Pierce, *Phys. Rev. D* **67**, 071702 (2003).
- [15] A. Finch, H. Nowak and A. Sopczak, in *Proc. of International Workshop on Linear Colliders (LCWS 2002)*, Jeju Island, Korea (26–30 Aug 2002) [hep-ph/0211140];  
A. Bartl, S. Hesselbach, K. Hidaka, T. Kernreiter and W. Porod, hep-ph/0306281.
- [16] A. Finch, A. Sopczak and H. Nowak, in *Prec. of the International Europhysics Conference on High-Energy Physics (HEP 2003)*, Aachen, Germany, 17-23 Jul 2003 [LC Note LC-PHSM-2003-075].
- [17] S. Y. Choi, J. S. Shim, H. S. Song and W. Y. Song, hep-ph/9808227;  
V. D. Barger, T. Falk, T. Han, J. Jiang, T. Li and T. Plehn, *Phys. Rev. D* **64**, 056007 (2001).
- [18] S. Y. Choi, A. Djouadi, M. Guchait, J. Kalinowski, H. S. Song and P. M. Zerwas, *Eur. Phys. J. C* **14**, 535 (2000).
- [19] B. C. Allanach *et al.*, *Eur. Phys. J. C* **25** (2002) 113.
- [20] S. Y. Choi, J. Kalinowski, G. Moortgat-Pick and P. M. Zerwas, *Eur. Phys. J. C* **22**, 563 (2001) [Addendum-*ibid.* C **23**, 769 (2002)].
- [21] R. Barate *et al.* [LEP2 Higgs Working Group, ALEPH, DELPHI, L3 and OPAL Collaborations], *Phys. Lett. B* **565**, 61 (2003);  
LEP2 Higgs Working Group, ALEPH, DELPHI, L3 and OPAL experiments, note LHWG-Note-2004-01. [<http://lephiggs.web.cern.ch/LEPHIGGS/papers/>].
- [22] A. Pilaftsis and C. E. M. Wagner, *Nucl. Phys. B* **553**, 3 (1999);  
A. Brignole, G. Degrossi, P. Slavich and F. Zwirner, *Nucl. Phys. B* **643**, 79 (2002);  
J. S. Lee, A. Pilaftsis, M. Carena, S. Y. Choi, M. Drees, J. R. Ellis and C. E. M. Wagner, *Comput. Phys. Commun.* **156**, 283 (2004);  
S. Heinemeyer, W. Hollik and G. Weiglein, hep-ph/0412214.
- [23] M. Carena, M. Quirós, M. Seco and C. E. M. Wagner, *Nucl. Phys. B* **650**, 24 (2003).
- [24] C. Balázs, M. Carena, A. Menon, D. E. Morrissey and C. E. M. Wagner, *Phys. Rev. D* **71**, 075002 (2005).
- [25] M. Carena, G. Nardini, M. Quirós and C. E. M. Wagner, in preparation.

- [26] M. Carena, M. Quirós, A. Riotto, I. Vilja and C. E. M. Wagner, Nucl. Phys. B **503**, 387 (1997);  
 J. M. Cline, M. Joyce and K. Kainulainen, JHEP **0007**, 018 (2000);  
 M. Carena, J. M. Moreno, M. Quirós, M. Seco and C. E. M. Wagner, Nucl. Phys. B **599**, 158 (2001).
- [27] T. Ibrahim and P. Nath, Phys. Rev. D **58**, 111301 (1998) [Erratum-ibid. D **60**, 099902 (1999)].
- [28] S. Abel, S. Khalil and O. Lebedev, Nucl. Phys. B **606**, 151 (2001).
- [29] B. C. Regan, E. D. Commins, C. J. Schmidt and D. DeMille, Phys. Rev. Lett. **88**, 071805 (2002).
- [30] K. i. Hikasa and M. Kobayashi, Phys. Rev. D **36**, 724 (1987).
- [31] T. Sjöstrand, P. Eden, C. Friberg, L. Lönnblad, G. Miu, S. Mrenna and E. Norrbin, Comput. Phys. Commun. **135**, 238 (2001);  
 see also T. Sjöstrand, L. Lönnblad and S. Mrenna, hep-ph/0108264.
- [32] A. Sopczak, in *Physics at LEP2*, eds. G. Altarelli, T. Sjöstrand and F. Zwirner, CERN 96-01, p. 343.
- [33] M. Pohl and H. J. Schreiber, hep-ex/0206009.
- [34] T. Kuhl, *N-Tuple working on Simdet DST structure*,  
<http://www.desy.de/~kuhl/ntuple/ntuple.html>.
- [35] A. Freitas, D. J. Miller and P. M. Zerwas, Eur. Phys. J. C **21** (2001) 361;  
 A. Freitas, A. von Manteuffel and P. M. Zerwas, Eur. Phys. J. C **34** (2004) 487.
- [36] F. Yuasa *et al.*, Prog. Theor. Phys. Suppl. **138**, 18 (2000).
- [37] E. Boos *et al.* [CompHEP Collaboration], Nucl. Instrum. Meth. A **534**, 250 (2004).
- [38] T. Ohl, Comput. Phys. Commun. **101**, 269 (1997).
- [39] K. Ackerstaff *et al.* [OPAL Collaboration], Eur. Phys. J. C **6**, 225 (1999);  
 G. Abbiendi *et al.* [OPAL Collaboration], Phys. Lett. B **545**, 272 (2002) [Erratum-ibid. B **548**, 258 (2002)].
- [40] T. Kuhl, in *Proc. of the International Conference on Linear Colliders (LCWS 04)*, Paris, France, 19-24 Apr 2004;  
 T. Kuhl, LC Note in preparation.
- [41] A. Bartl, H. Eberl, S. Kraml, W. Majerotto, W. Porod and A. Sopczak, Z. Phys. C **76**, 549 (1997).

- [42] G. Moortgat-Pick *et al.*, *The Role of Polarized Positrons and Electrons in Revealing Fundamental Interactions at the Linear Collider*, working group report of the *POWER* working group, hep-ph/0507011.
- [43] M. Winter, LC Note LC-PHSM-2001-016.
- [44] A. Denner, S. Dittmaier, M. Roth and L. H. Wieders, *Phys. Lett. B* **612**, 223 (2005).
- [45] I. Foresti and H. Nowak, L3 Internal Note 2301 (1998).
- [46] K. Mönig, in *Proc. of the 2nd ECFA/DESY Linear Collider Study (1998-2001)*, p. 1353-1361 [LC Note LC-PHSM-2000-060].
- [47] K. Desch, J. Kalinowski, G. Moortgat-Pick, M. M. Nojiri and G. Polesello, *JHEP* **0402**, 035 (2004).
- [48] *ATLAS Detector and Physics Performance Technical Design Report, Vol 2.*, CERN-LHCC-99-15 (1999).
- [49] T. Krupovnickas, talk given at the Argonne Theory Institute, Argonne, Illinois, 9-13 May 2005.
- [50] A. Freitas, H. U. Martyn, U. Nauenberg and P. M. Zerwas, in *Proc. of the International Conference on Linear Colliders (LCWS 04), Paris, France, 19-24 Apr 2004* [hep-ph/0409129].
- [51] H. U. Martyn, LC Note LC-PHSM-2003-071.
- [52] LHC/ILC Study Group Working Report, eds. G. Weiglein *et al.*, hep-ph/0410364.
- [53] R. Hawkings, LC Note LC-PHSM-2000-021;  
S. M. Xella-Hansen, M. Wing, D. J. Jackson, N. de Groot and C. J. S. Damerell, LC Note LC-PHSM-2003-061;  
K. Desch, T. Klimkovich, T. Kuhl and A. Raspereza, LC Note LC-PHSM-2004-006.
- [54] V. D. Barger and T. Han, *Phys. Lett. B* **212** (1988) 117;  
V. D. Barger, T. Han and R. J. Phillips, *Phys. Rev. D* **39** (1989) 146;  
A. Tofghi-Niaki and J. F. Gunion, *Phys. Rev. D* **39** (1989) 720.
- [55] U. Nauenberg, talk given at the ECFA/DESY Linear Collider workshop, Prague, 15–18 Nov 2002.
- [56] M. Ball, Diplom thesis, University of Hamburg (2003),  
<http://www-flc.desy.de/thesis/diplom.2002.ball.ps.gz>,  
see also talk by K. Desch at the ECFA/DESY Linear Collider workshop, Prague, 15–18 Nov 2002.
- [57] J. F. Gunion, T. Han, J. Jiang and A. Sopczak, *Phys. Lett. B* **565**, 42 (2003).

- [58] P. Garcia-Abia, W. Lohmann and A. Raspereza, in *Proc. of the 5th International Linear Collider Workshop (LCWS 2000)*, Fermilab, Batavia, Illinois, 24-28 Oct 2000 [LC Note LC-PHSM-2000-062].
- [59] P. Garcia, W. Lohmann and A. Raspereza, in *Proc. of the 2nd ECFA/DESY Linear Collider Study (1998-2001)*, p. 2227–2235 [LC Note LC-PHSM-2001-054].
- [60] K. Desch and M. Battaglia, in *Proc. of the 5th International Linear Collider Workshop (LCWS 2000)*, Fermilab, Batavia, Illinois, 24-28 Oct 2000 [LC Note LC-PHSM-2001-053].
- [61] H. Baer, C. Balázs and A. Belyaev, *JHEP* **0203**, 042 (2002).
- [62] A. Finch, H. Nowak and A. Sopczak, in *Proc. of the International Conference on Linear Colliders (LCWS 04)*, Paris, France, 19-24 Apr 2004;  
H. Nowak, A. Finch and A. Sopczak, to appear in *Proc. of the International Linear Collider Workshop (LCWS 05)*, Stanford, California, USA, 18-22 Mar 2005.
- [63] M. Schmitt, *A Technique for Extracting Masses with Reduced Systematics*, in preparation.